

Apelin treatment increases complete Fatty Acid oxidation, mitochondrial oxidative capacity, and biogenesis in muscle of insulin-resistant mice.

Camille Attané, Camille Foussal, Sophie Le Gonidec, Alexandre Benani, Danièle Daviaud, Estelle Wanecq, Rocío Guzmán-Ruiz, Cédric Dray, Veronic Bezaire, Chloé Rancoule, et al.

▶ **To cite this version:**

Camille Attané, Camille Foussal, Sophie Le Gonidec, Alexandre Benani, Danièle Daviaud, et al.. Apelin treatment increases complete Fatty Acid oxidation, mitochondrial oxidative capacity, and biogenesis in muscle of insulin-resistant mice.. Diabetes, 2012, 61 (2), pp.310-20. 10.2337/db11-0100 . hal-00723095

HAL Id: hal-00723095

https://u-bourgogne.hal.science/hal-00723095

Submitted on 29 May 2020

HAL is a multi-disciplinary open access archive for the deposit and dissemination of scientific research documents, whether they are published or not. The documents may come from teaching and research institutions in France or abroad, or from public or private research centers.

L'archive ouverte pluridisciplinaire **HAL**, est destinée au dépôt et à la diffusion de documents scientifiques de niveau recherche, publiés ou non, émanant des établissements d'enseignement et de recherche français ou étrangers, des laboratoires publics ou privés.



Distributed under a Creative Commons Attribution - NonCommercial - NoDerivatives 4.0 International License

Apelin Treatment Increases Complete Fatty Acid Oxidation, Mitochondrial Oxidative Capacity, and Biogenesis in Muscle of Insulin-Resistant Mice

Camille Attané,[1,2] Camille Foussal,[1,2] Sophie Le Gonidec,[1,2] Alexandre Benani,[3] Danièle Daviaud,[1,2] Estelle Wanecq,[1,2] Rocío Guzmán-Ruiz,[4] Cédric Dray,[1,2] Veronic Bezaire,[1,2] Chloé Rancoule,[1,2] Keiji Kuba,[5] Mariano Ruiz-Gayo,[4] Thierry Levade,[1,2] Josef Penninger,[6] Rémy Burcelin,[1,2] Luc Pénicaud,[3] Philippe Valet,[1,2] and Isabelle Castan-Laurell[1,2]

Both acute and chronic apelin treatment have been shown to improve insulin sensitivity in mice. However, the effects of apelin on fatty acid oxidation (FAO) during obesity-related insulin resistance have not yet been addressed. Thus, the aim of the current study was to determine the impact of chronic treatment on lipid use, especially in skeletal muscles. High-fat diet (HFD)-induced obese and insulin-resistant mice treated by an apelin injection (0.1 μmol/kg/day i.p.) during 4 weeks had decreased fat mass, glycemia, and plasma levels of triglycerides and were protected from hyperinsulinemia compared with HFD PBS-treated mice. Indirect calorimetry experiments showed that apelin-treated mice had a better use of lipids. The complete FAO, the oxidative capacity, and mitochondrial biogenesis were increased in soleus of apelin-treated mice. The action of apelin was AMP-activated protein kinase (AMPK) dependent since all the effects studied were abrogated in HFD apelin-treated mice with muscle-specific inactive AMPK. Finally, the apelin-stimulated improvement of oxidative capacity led to decreased levels of acylcarnitines and enhanced insulin-stimulated glucose uptake in soleus. Thus, by promoting complete lipid use in muscle of insulin-resistant mice through mitochondrial biogenesis and tighter matching between FAO and the tricarboxylic acid cycle, apelin treatment could contribute to insulin sensitivity improvement. ***Diabetes*** **61:310–320, 2012**

Apelin is a circulating peptide, present in different tissues but also produced and secreted by human and mouse adipocytes (1). Apelin was identified as the endogenous ligand of the ubiquitously expressed G protein–coupled receptor named APJ (2). The apelin/APJ system exerts a large number of physiological roles, including regulation of fluid homeostasis, cardiovascular, immune, and gastrointestinal functions (3). A role for apelin/APJ in energy metabolism also has emerged recently. Acute and chronic apelin treatment has been shown to regulate glucose homeostasis (4,5). Beneficial effects of acute intravenous injection of apelin were observed in normal-chow diet (ND)-fed mice on glucose uptake, especially in skeletal muscle, through an AMP-activated protein kinase (AMPK)-dependent pathway (5). It is interesting that obese and insulin-resistant mice, exhibiting higher plasma apelin concentration than ND-fed mice (6), benefit from an acute apelin treatment since glucose tolerance was improved and muscle glucose uptake increased during a euglycemic-hyperinsulinemic clamp (5). Chronic apelin treatment also ameliorates insulin sensitivity in young *db/db* mice (5). Conversely, apelin KO mice develop insulin resistance especially when fed a high-fat diet (HFD) (5). Altogether, these studies support a physiological role for apelin in the regulation of glucose homeostasis. Chronic apelin treatment also decreases lipid storage in adipose tissue since a reduction of triglycerides (TGs) in various fat depots has been observed in ND- and HFD-fed mice (7). Paradoxically, acute apelin treatment has been shown very recently to inhibit lipolysis in isolated adipocytes of non-obese mice (8) but not in human adipose tissue (9). The fate of lipids mobilized by chronic apelin treatment in obese and insulin-resistant mice is thus still unclear. More specific, the effects of apelin on fatty acid oxidation (FAO) have not yet been addressed.

To understand the impact of apelin on lipid metabolism, this study was designed on both in vivo and ex vivo approaches in obese and insulin-resistant mice chronically treated (or not) with apelin. Our data show that in apelin-treated obese and insulin-resistant mice, the main whole-body substrates oxidized in vivo were lipids. Ex vivo, in muscle of insulin-resistant mice, apelin treatment increased complete FAO, oxidative phosphorylation, and mitochondrial biogenesis but also increased insulin sensitivity by decreasing acylcarnitine levels and stimulating glucose uptake.

RESEARCH DESIGN AND METHODS

Mice were handled in accordance with the principles and guidelines established by INSERM. C57Bl6/J wild-type (WT) mice were obtained from Harlan (Gannat, France). Mice with muscle-specific inactive AMPK (AMPK-DN mice) were provided by Prof. Moris J. Birnbaum (Howard Hughes Medical Institute, University of Pennsylvania, Philadelphia, PA). Apelin-deficient (apelin$^{-/-}$) mice were generated as described previously (10) and backcrossed to C57Bl6/J mice >10 times. Mice were housed conventionally in a constant temperature (20–22°C) and humidity (50–60%) animal room, with a 12/12 h light/dark cycle (lights on at 7:00 A.M.) and free access to food and water. The C57Bl6/J and AMPK-DN mice were fed an ND from weaning until aged 10 weeks and then either maintained on ND (control group) or fed an HFD containing 20%

From [1]INSERM U1048, Toulouse, France; the [2]Université de Toulouse, Université Paul Sabatier, Institut des Maladies Métaboliques et Cardiovasculaires (I2MC), Toulouse, France; the [3]Centre des Sciences du Goût et de l'Alimentation, Unité Mixte de Recherche 6265–Centre National de la Recherche Scientifique 13241–Institut National de la Recherche Agronomique, Université de Bourgogne, Dijon, France; the [4]Departemento de Ciencias Farmacéuticas y de la Alimentación, School of Pharmacy, University CEU–San Pablo, Madrid, Spain; the [5]Department of Biological Informatics and Experimental Therapeutics, Akita University Graduate School of Medicine, Akita, Japan; and the [6]Institute of Molecular Biotechnology, Vienna, Austria.

Corresponding author: Isabelle Castan-Laurell, isabelle.castan@inserm.fr.

Received 26 January 2011 and accepted 27 November 2011.

DOI: 10.2337/db11-0100

This article contains Supplementary Data online at http://diabetes.diabetesjournals.org/lookup/suppl/doi:10.2337/db11-0100/-/DC1.

© 2012 by the American Diabetes Association. Readers may use this article as long as the work is properly cited, the use is educational and not for profit, and the work is not altered. See http://creativecommons.org/licenses/by-nc-nd/3.0/ for details.

protein, 35% carbohydrate, and 45% fat (Research Diets, New Brunswick, NJ). Apelin treatment began after the onset of insulin resistance in males aged 23 weeks. Mice were injected daily with apelin-13 (Phoenix Biotech) at 0.1 μmol/kg/day i.p. as previously described (7) for 28 days. Age-matched control mice were PBS injected during the same period. Standard mice were also treated with a specific APJ receptor antagonist (F13A) (Phoenix Biotech) (11) at 0.2 μmol/kg/day during 28 days or with the combination of apelin and F13A. All mice were killed 24 h after the last apelin injection in a fed state. Plasma apelin concentrations, measured after a bolus of apelin (0.1 μmol/kg i.p.) in HFD mice, were increased >2.4-fold 10 min after injection (4.12 ± 0.96 vs. 1.73 ± 0.24 ng/mL before the injection, $n = 5$), but plasma apelin concentrations were not different between PBS- and apelin-treated mice at the end of the treatment (Table 1).

Body fat mass composition. To determine fat and lean mass, mice were placed in a clear plastic holder, without anesthesia or sedation, and inserted into the EchoMRI-3-in-1 system (Echo Medical Systems, Houston, TX). Total body fat and lean mass were measured before (day 0) and at the end of the treatment (day 28) in apelin- and PBS-treated mice.

Plasma measures. Plasma fatty acids (FAs) and TGs measured by colorimetric technique with the Wako NEFA kit (Wako Chemicals) and the PAP 150 Kit (bioMerieux), respectively, as well as plasma leptin, adiponectin (Quantikine; R&D Systems), and apelin (Phoenix Pharmaceuticals, Inc.), were determined in the fed state at the end of the treatment. Insulinemia (Mercodia, Uppsala, Sweden) and glycemia measured with a glucometer (Accu-check; Roche Diagnostics) were determined in the fasted state on blood from the tail vein.

Glucose and insulin tolerance tests. Glucose and insulin tolerance tests (GTT and ITT, respectively) were performed before apelin treatment and 1 week before the end of the treatment. Mice were fasted for 6 h and were then injected with glucose (1 g/kg i.p.), and blood glucose levels from the vein tail were monitored over time using a glucometer as previously described (4). For the ITT, mice were injected with insulin (0.75 units/kg) and blood glucose levels were measured as in the GTT.

Whole-body indirect calorimetry. Indirect calorimetry was performed between the 3rd and 4th week of treatment after 24 h of acclimatization. O_2 consumption (V_{O_2}) and CO_2 production (V_{CO_2}) were measured (Oxylet; Panlab-Bioseb, Vitrolles, France) in individual mice at 25 min intervals during a 24-h period. The respiratory exchange ratio ([RER] = V_{CO_2}/V_{O_2}) was measured. Energy expenditure (in kcal/day/kg$^{0.75}$ = $1.44 \times V_{O_2} \times [3.815 + 1.232 \times \text{RER}]$), glucose oxidation (in g/min/kg$^{0.75}$ = $[(4.545 \times V_{CO_2}) - (3.205 \times V_{O_2})]/1000$), and lipid oxidation (in g/min/kg$^{0.75}$ = $[1.672 \times (V_{O_2} - V_{CO_2})]/1000$) were calculated. Ambulatory activities of the mice were monitored by an infrared photocell beam interruption method (Sedacom; Panlab-Bioseb).

Palmitate oxidation and esterification. Palmitate oxidation was determined as previously described in whole soleus muscle or adipose tissues (12). The tissues were incubated in modified Krebs-Henseleit buffer containing 1.5% FA-free BSA, 5 mmol/L glucose, 1 mmol/L palmitate, and 0.5 μCi/mL [^{14}C] palmitate (PerkinElmer) for 60 min. At the end of the incubation, tissues were removed and homogenized in 800 μL lysis buffer. Complete oxidation was determined by acidifying the incubation buffer with 1 mL of 1 mol/L H_2SO_4, and the $^{14}CO_2$ was trapped by benzethonium hydroxide (Sigma-Aldrich) placed in a 0.5 mL microtube in a sealed glass vial. After 120 min, the microtube was removed and placed in a scintillation vial, and the radioactivity was counted (Cytoscint; MP Biomedicals). A total of 500 μL homogenate was placed into glass tubes to extract lipids with chloroform-methanol (2:1) and 2 mol/L KCl-HCl. After centrifugation, the aqueous phase (500 μL) was quantified by liquid scintillation to determine the acid-soluble metabolites production (incomplete oxidation) and the organic phase (200 μL) used to measure palmitate esterification as previously described (12).

O_2 consumption measurement on mitochondria. O_2 consumption was measured on fresh permeabilized fibers prepared from soleus muscle using a respirometer (Oxygraph-2k; OROBOROS INSTRUMENTS, Innsbruck, Austria) as previously described (13,14). First, a 20 mmol/L glutamate per 4 mmol/L malate mixture was injected to assess the complex I activity (gmState 2). Complex I was then blocked by addition of 5 μmol/L rotenone. Thereafter, 10 mmol/L succinate was added to access the complex II activity (sState 2). State 3 of respiration was obtained after further addition of 10 mmol/L ADP. O_2 consumption for each state was calculated using DataGraph software.

Transmission electron microscopy. Soleus muscle was cut into small pieces and fixed as previously reported (15). The tissue was then cut and mounted on copper grids and observed with a Hitachi HU 12A transmission electron microscope equipped with a high-resolution camera. The pictures obtained were analyzed with Lucia G software.

Mitochondrial DNA analysis. Total DNA was extracted from soleus muscle using a commercial kit (DNeasy; QIAGEN). The content of mitochondrial (mt) DNA was calculated using real-time quantitative PCR by measuring the threshold cycle ratio of a mitochondrial encoded gene (*COX1*) and a nuclear-encoded gene (cyclophilin A) as previously described (15).

TABLE 1
Body weight, fat mass, and plasma parameters measured in HFD-fed mice treated or not with apelin

	Treatment	
	PBS (n = 13)	Apelin (n = 12)
Body weight after treatment (g)	44. 1 ± 0.9	44.8 ± 0.9
Weight gain (g)	−0.22 ± 0.32	−0.36 ± 0.35
Fat mass (%) after treatment	35.79 ± 1.30	34.32 ± 1.36
Whole-body fat gain (%)	1.42 ± 0.51	−0.11 ± 0.57*
Plasma FA (mmol/L)	0.33 ± 0.01	0.33 ± 0.02
Plasma TG (g/L)	0.87 ± 0.04	0.71 ± 0.04*
Plasma apelin (ng/mL)	1.48 ± 0.11	1.36 ± 0.06
Plasma adiponectin (μg/mL)	13.49 ± 0.86	14.17 ± 2.53
Plasma leptin (ng/mL)	153 ± 17	141 ± 23

Data are means ± SEM. The percentage of fat mass corresponds to the ratio between fat mass (g) and body weight (g) × 100. Whole-body fat gain corresponds to the difference in percent fat after and before the treatment. *$P \leq 0.05$ vs. PBS-treated mice.

Citrate synthase assay. Citrate synthase was measured on frozen soleus muscle as previously described (16). In brief, muscle tissue was homogenized (10 mg tissue/500 μL buffer) on ice with a potter in buffer containing 0.1 mol/L KH_2PO_4 and 0.05% BSA (pH 7.3 at 4°C), and the assay was done on 10 μL homogenate.

Determination of skeletal muscle acylcarnitines, diacylglycerol, and TG levels

Acylcarnitines. Part of muscle homogenate (20 μL) was spotted on filter membranes (Protein Saver 903 cards; Whatman). The dried spots were then treated as reported (17). In brief, acylcarnitines were derivatized by addition of butanolic HCl and treated with the reagents of the NeoGram MSMS-AAAC kit (PerkinElmer). Free carnitine and acylcarnitines were quantified by liquid chromatography–tandem mass spectrometry. Data were acquired using a Micromass Quattro Micro API spectrometer equipped with a 2795 high-performance liquid chromatography module and a data system controlled by MassLynx 4.1 operating system (Waters, Milford, MA).

Neutral lipids (diacylglycerol and TG). Muscles (5–10 mg) were homogenized in 2 mL methanol per 5 mmol/L EGTA (2:1 v/v) with FAST-PREP (MP Biomedicals). A total of 100 μL was evaporated, the dry pellets were dissolved in 0.1 mL NaOH (0.1 mol/L) overnight, and proteins were measured with the Bio-Rad assay. Neutral lipids corresponding to 0.9 mL of the homogenate were extracted according to Bligh and Dyer (18) in chloroform/methanol/water (2.5:2.5:2.1 v/v/v) in the presence of the internal standards and measured as previously described (19).

Malonyl-CoA assay. Malonyl-CoA levels were measured on frozen soleus muscle as previously described (20). In brief, muscle were homogenized (10 mg tissue in 250 μL phosphate buffer containing 1 mol/L KPO_4 and 10 mmol/L EDTA, pH 7.0) on ice with a potter and then centrifuged. Supernatant (100 μL) was then incubated for 1 h at 37°C with assay buffer (phosphate buffer with 2.5 mmol/L dithiothreitol, 0.2 mmol/L NADPH, 0.01% free FA BSA, 13 μmol/L acetyl-CoA, and 0.63 μCi ^{3}H-acetyl-CoA) (PerkinElmer), and 25 mU of FA synthetase (provided by Prof. Marc Prentki, Centre Hospitalier de l'Université de Montréal Research Centre, Montreal, Ontario, Canada). The reaction stopped with 25 μL perchloric acid, and then ethanol and petroleum acid was added. A total of 4 mL of the upper phase was transferred in a new tube containing 2 mL water, and after centrifugation, 3 mL of the upper phase was dried and radioactivity was measured after addition of 10 mL scintillation liquid.

Western blot analysis. Western blot analyses were performed as previously described (4) by loading samples (lysed muscle) on 4–12% Criterion/XT gel (Bio-Rad) and transferring to nitrocellulose membranes (Schleicher & Schuell Bioscience) that had been probed with antiphospho–AMPK-α (Thr172), antiphospho–acetyl-CoA carboxylase (ACC) (Ser79) (Cell Signaling Technology, Beverly, MA), or anti-OxPhos antibodies (MitoSciences, Mundolsheim, France) used at 1/1,000 dilution. Membranes were probed with β-actin or AMPK or ACC antibodies for total proteins.

Protein assay. Concentration of samples was determined using the DC protein assay kit (Bio-Rad) according to the manufacturer's instructions.

Real-time PCR. Total RNAs (1 μg) were isolated from muscle using RNA STAT (AMS Technology, Lutterworth, U.K.) and were reverse transcribed using random hexamers and Superscript II reverse transcriptase (Invitrogen, Paisley, U.K.). Real time PCR was performed as previously described (1). Analysis of the 18S ribosomal RNA was performed using the ribosomal RNA control TaqMan Assay Kit (Applied Biosystems) to normalize gene expression.

Glucose uptake. Muscles were isolated and preincubated for 10 min in Krebs-Henseleit buffer (pH 7.4) containing 2 mg/mL BSA, 2 mmol/L sodium pyruvate, and 20 mmol/L HEPES. Muscles were then incubated for 45 min in the absence or presence of 100 nmol/L insulin as previously reported (4).

Lipolysis. Lipolysis was measured after collagenase digestion of white adipose tissue (WAT) from PBS- and apelin-treated mice as previously reported (21). In brief, isolated adipocytes were incubated in the presence (or not) of different concentrations of isoprenaline (a β-adrenergic agonist). Glycerol released in the medium was measured on 30 μL aliquot using the Glycerol Free Reagent kit (Sigma-Aldrich).

Statistical analysis. Data are presented as means ± SEM. Comparisons between groups were carried out for different parameters using Prism 5.0 software (GraphPad Software). A two-way ANOVA was applied to detect interaction between treatment and time. When appropriate, Student *t* test paired or nonpaired was applied. Differences at $P < 0.05$ were considered statistically significant.

RESULTS

Effect of chronic apelin treatment in vivo in HFD-fed mice. HFD-fed mice were obese and insulin resistant before apelin treatment. At the end of apelin treatment, HFD mice had significant lower blood glucose and were protected from hyperinsulinemia compared with HFD PBS-treated mice (Fig. 1*A*). HFD apelin-treated mice also had significantly reduced adiposity and plasma levels of TG, whereas FA levels and leptin and adiponectin plasma concentrations were not modified (Table 1). Moreover, apelin-treated mice were significantly more responsive to glucose and insulin at the end of the treatment (Fig. 1*B* and *C*). To determine whether this improvement of insulin sensitivity was due to a change in substrate use, indirect calorimetry was performed.

During the 24-h experiment, food intake and physical activity were not modified between PBS- and apelin-treated mice (Table 2). V_{O_2} and energy expenditure tended to increase with apelin treatment, whereas V_{CO_2} values were similar (Table 2). However, apelin-treated mice clearly exhibited a lower RER, especially during the feeding period (dark cycle) compared with PBS-treated mice (Fig. 2*A* and *B*), indicative of a higher use of lipids. These results were confirmed by the calculated amount of lipid oxidized, which was increased, whereas the amount of glucose oxidized was decreased in HFD apelin-treated mice (Fig. 2*C*).

To determine the impact of apelin per se on whole-body substrate use, indirect calorimetry was performed in apelin$^{-/-}$ mice. Apelin$^{-/-}$ mice fed an HFD for 12 weeks had increased fat mass (39.41 ± 1.71 [n = 9] vs. 35.05 ± 0.88% in WT HFD mice [n = 12]; $P < 0.02$) and were insulin resistant (area under the curve for ITT: 8,814.2 ± 256.7 vs. 6,200 ± 439.6 arbitrary units in WT HFD mice, n = 12; $P < 0.001$). The RER of HFD apelin $^{-/-}$ mice was similar to HFD WT mice during the dark period and did not decrease during the light period (Supplementary Fig. 1). This translated to increased glucose oxidation and decreased lipid oxidation during the light period in HFD apelin $^{-/-}$ mice compared with HFD WT mice.

Effect of chronic apelin treatment in HFD mice on skeletal muscle lipid metabolism ex vivo. Since more lipids were used in whole-body organism of HFD apelin-treated mice, lipid metabolism in skeletal muscle was studied. As expected, muscle homogenates of HFD mice contained higher levels of diacylglycerol (DAG) (ND: 11.98 ± 2.74 nmol/mg protein, n = 5; HFD: 84.03 ± 10.97 nmol/mg protein, n = 7) and intramuscular TG (IMTG) (ND: 163.7 ± 41.4 nmol/mg protein, n = 5; HFD: 182.3 ± 23.2 nmol/mg protein,

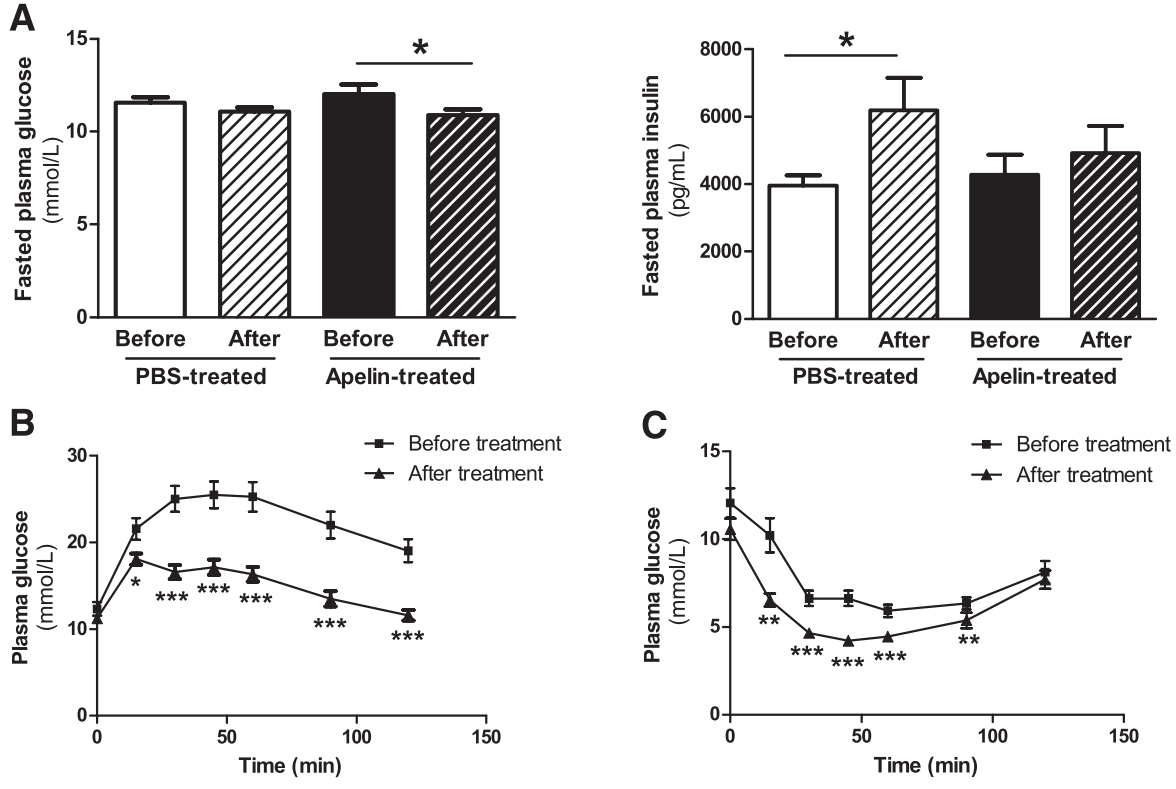


FIG. 1. Chronic apelin treatment in HFD mice improved insulin sensitivity. *A*: Fasted glucose (*left*) and insulin blood levels (*right*) in PBS-treated (control, n = 12) and apelin-treated (n = 12) mice before and after the treatment. Results are means ± SEM. *$P \le 0.05$. *B*: GTT before and at the end of the apelin treatment in HFD mice (n = 12). *C*: ITT before and at the end of the apelin treatment in HFD mice (n = 8). Results are means ± SEM. *$P \le 0.05$, **$P \le 0.01$, ***$P \le 0.001$.

TABLE 2
Indirect calorimetry parameters measured in HFD PBS- and apelin-treated mice

	Treatment	
	PBS (n = 13)	Apelin (n = 12)
Dark period		
V_{CO_2} (mL/g/h)	23.10 ± 0.95	23.68 ± 1.20
V_{O_2} (mL/g/h)	31.07 ± 1.15	33.94 ± 1.65
EE (kcal/h)	211.7 ± 7.9	224.1 ± 10.3
Light period		
V_{CO_2} (mL/g/h)	21.05 ± 0.80	22.62 ± 1.18
V_{O_2} (mL/g/h)	29.56 ± 1.10	32.60 ± 1.58
EE (kcal/h)	199.9 ± 7.5	214.6 ± 10.8
Light and dark period		
Food intake (g)	2.99 ± 0.3	2.68 ± 0.45
Activity (beam breaks/5 min)	91 ± 15	72 ± 19

Data are means ± SEM. V_{CO_2} and V_{O_2} values represent the average values recorded during the period. EE, energy expenditure.

n = 7) compared with ND mice. However, apelin treatment in HFD mice was unsuccessful in reducing the amount of IMTG and DAG when compared with PBS treatment (Fig. 3*A*). Apelin treatment also had no effect on the rate of palmitate incorporation into TG (Fig. 3*B*). To further investigate the fates of lipids, both complete and incomplete oxidation of [^{14}C]palmitate were assessed. Chronic apelin treatment significantly increased complete oxidation of [^{14}C]palmitate to CO_2 in soleus muscle when compared with PBS treatment (Fig. 3*C*). Of interest, incomplete oxidation was not significantly increased by chronic apelin treatment (Fig. 3*C*). Moreover, in soleus of HFD apelin$^{-/-}$ mice, the complete oxidation was not increased (243.5 ± 9.6 vs. 198.4 ± 59.9 nmol CO_2 released per gram protein in apelin$^{-/-}$ mice, n = 3–4). Altogether, these results show that apelin treatment promotes complete FAO rather than accumulation of TG or partially oxidized FA in skeletal muscle of obese and insulin-resistant mice. The effect of apelin treatment on FAO seems restricted to skeletal muscle since no significant metabolic changes were observed in brown adipose tissue and WAT (Supplementary Fig. 2).

Effect of chronic apelin treatment in HFD mice on muscle mitochondrial activity and density. To get further insight toward the effect of apelin, mitochondrial respiration was first assessed on freshly permeabilized muscle fibers. No difference in the glutamate/malate–driven mitochondrial respiration was found between PBS- and apelin-treated mice, suggesting that the complex I activity was not affected by the apelin treatment (data not shown). However, the succinate-driven mitochondrial respiration was significantly higher in fibers from apelin-treated mice compared with control, suggesting an increase in the oxidative capacity from complex II that uses coenzymes derived from FAO (Fig. 4*A*). The succinate and adenylate-driven respiration was also significantly higher in apelin-treated mice, indicating that the capacity of the oxidative phosphorylation was increased in soleus after apelin treatment. Protein expression of complex II, III, and V also was significantly increased in apelin-treated mice (Fig. 4*B*). In addition, an increased citrate synthase activity, a quantitative marker of mitochondria content, was also found in muscle homogenates of apelin-treated mice compared with control (2.62 ± 0.02 vs. 2.91 ± 0.07 μmol/min/mg proteins, n = 7–9; $P < 0.001$). Expression of peroxisome proliferator–activated receptor γ coactivator 1-α (PGC1-α), a transcriptional coactivator mediating mitochondrial biogenesis (22), was also significantly increased in muscle of apelin-treated mice, whereas expression of PGC1-β was not modified (Fig. 4*C*). Moreover, expression of nuclear respiratory factor 1 (NRF1) and mitochondrial transcription factor A (TFAM), which act in concert to increase mitochondrial oxidative phosphorylation and mitochondrial biogenesis (23), were also upregulated. Altogether, these results strongly suggest that in response to apelin treatment, mitochondrial biogenesis was increased in skeletal muscle from insulin-resistant mice. To test this hypothesis, we measured muscle mtDNA and density. The mtDNA–to–nuclear DNA ratio was significantly higher in soleus muscle of apelin-treated mice than in PBS-treated mice (Fig. 4*D*). Moreover, the electron microscopy demonstrated that apelin treatment significantly increased the density of intramyofibrillar (IMF) mitochondria (Fig. 4*E*), the largest fraction of the total mitochondria content. Fewer adverse alterations of mitochondria ultrastructure (reduced electron density of the matrix and loss of cristae) also were observed in both IMF and subsarcolemmal (SS) mitochondria of soleus muscle of apelin-treated mice (Fig. 4*E*), strengthening the effect of apelin on mitochondria function and biogenesis.

To study more deeply the apelin mechanism of action, the involvement of APJ receptor in apelin effects was first determined. For this purpose, mice were treated during the same period with either apelin alone or apelin and a specific APJ receptor antagonist (F13A) (11). F13A/apelin–treated mice were glucose intolerant and had increased body weight, fat gain, and higher glycemia and insulinemia compared with apelin-treated mice (Supplementary Fig. 3). Thus, F13A antagonist behaved as a functional antagonist. In muscle of F13A/apelin–treated mice, FAO and mitochondrial biogenesis were abrogated compared with apelin-treated mice (Supplementary Fig. 3), indicating that apelin exerts its beneficial effects through APJ activation.

Next, the role of AMPK in mediating the effects of apelin was investigated since apelin is known to activate AMPK in skeletal muscle (4) and AMPK is involved in both FAO (24) and mitochondrial biogenesis (25). Apelin treatment significantly increased both AMPK and ACC phosphorylation in muscle of insulin-resistant mice (Fig. 5*A*). The inhibition of ACC activity (as a result of increased phosphorylation) had for consequence a significant reduction of malonyl-CoA concentrations in muscle of apelin-treated mice (Fig. 5*B*). In addition, the increased FAO and mitochondrial biogenesis observed in HFD WT apelin-treated mice was completely blunted in muscle of HFD AMPK-DN apelin-treated mice, and the overexpression of PGC1-α, TFAM, and NRF1 was reduced (Fig. 5*C–E*). Thus, AMPK is a direct target of apelin and is required for apelin effect on FAO and mitochondrial biogenesis.

Chronic apelin treatment in HFD mice improves muscle insulin sensitivity. Acylcarnitines represent by-products of substrate catabolism arising from incomplete FAO. Increased acylcarnitine levels have been shown to be associated with obesity and insulin resistance (26,27). Long-chain acylcarnitines were elevated in homogenates of soleus muscle from HFD insulin-resistant mice compared with ND control mice (Fig. 6*A*). It is interesting that in HFD apelin-treated mice, acylcarnitine levels, especially C16:1 and C18:1 species, were reduced when compared with HFD PBS-treated mice. Since chronic apelin

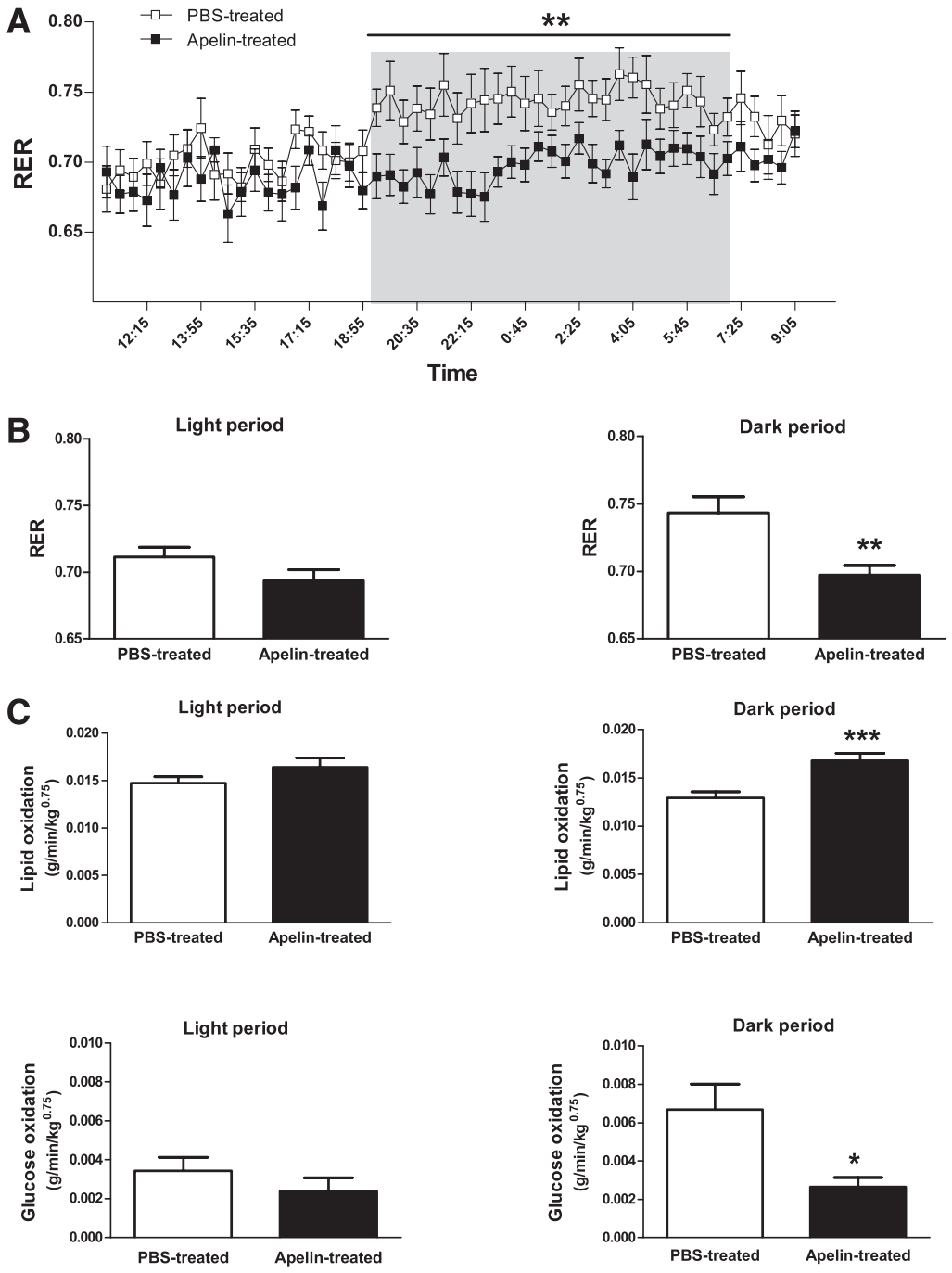


FIG. 2. Chronic apelin treatment in HFD mice increased lipid oxidation in vivo. *A*: RER measurement during 24 h in insulin-resistant mice chronically treated with PBS (n = 13) or apelin (n = 12). *B*: RER during the light and dark periods in PBS- (n = 13) and apelin-treated (n = 12) mice. *C*: Amount of lipid and glucose oxidized during the light and dark periods calculated as described in RESEARCH DESIGN AND METHODS in PBS- and apelin-treated mice. Results are means ± SEM. *$P \leq 0.05$, **$P \leq 0.01$, ***$P \leq 0.001$.

treatment increased complete but not incomplete FAO in soleus, we hypothesized that the resulting lower levels of acylcarnitines would correlate with improved insulin sensitivity in muscle. Indeed, insulin-stimulated glucose uptake was significantly increased in apelin-treated mice muscle compared with PBS-treated mice (Fig. 6*B*).

DISCUSSION

Insulin resistance is a major metabolic abnormality leading to type 2 diabetes. There is considerable interest in the discovery of insulin-sensitizing agents and in the development of new therapeutic strategies. The current study shows for the first time that chronic apelin treatment increases complete FAO, mitochondrial respiratory capacity, and mitochondrial biogenesis in skeletal muscle of insulin-resistant mice. The influx of lipid in mitochondria was associated with decreased acylcarnitine levels, suggesting a tighter coupling between FAO and the tricarboxylic acid cycle. Such a tighter coupling appears important to improve insulin sensitivity since increased insulin-stimulated glucose transport in muscle of apelin-treated mice is

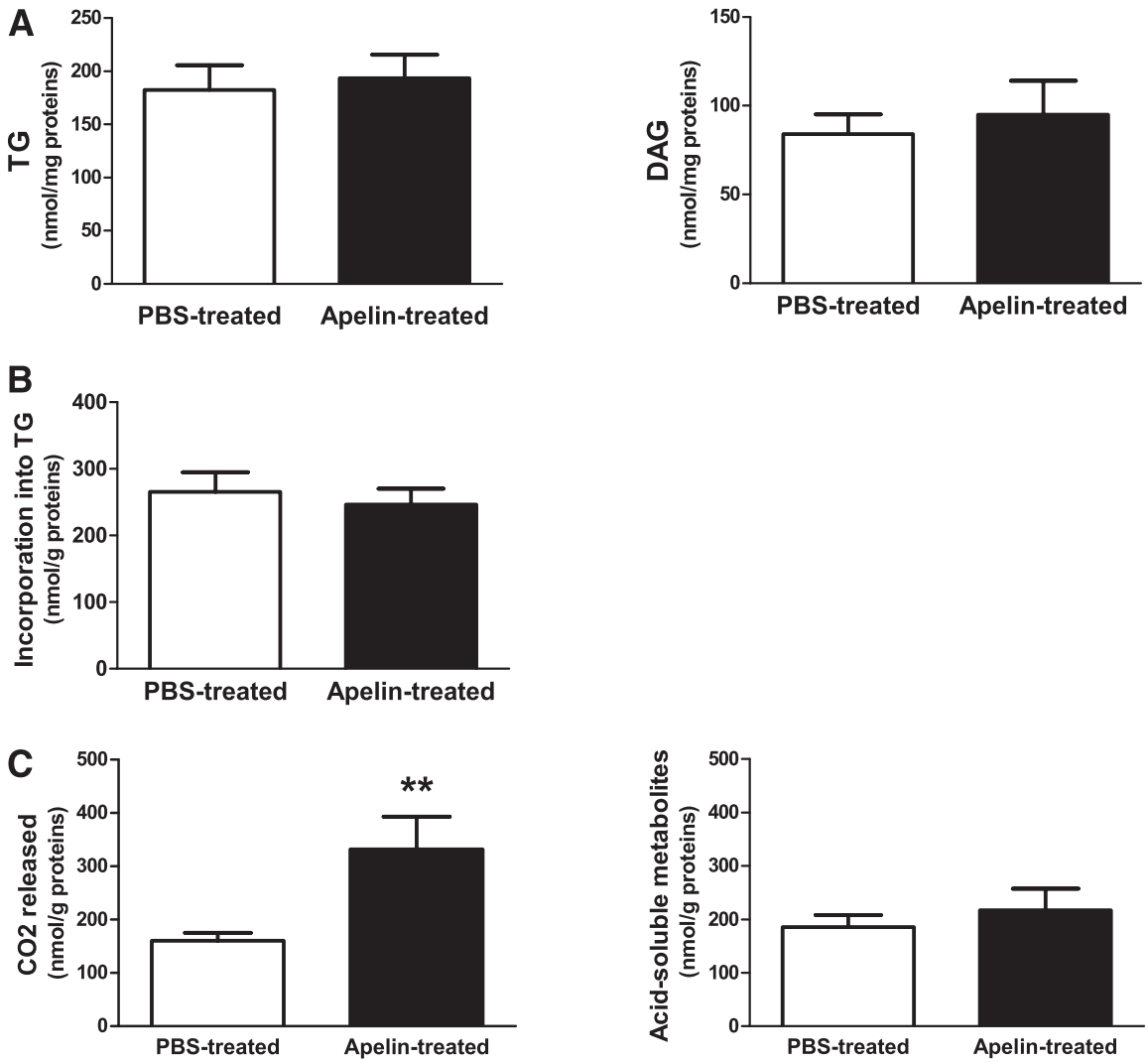


FIG. 3. Effect of chronic apelin treatment on palmitate partitioning in muscle of insulin-resistant mice. *A*: TG and DAG levels in muscle homogenates of PBS-treated (n = 7) and apelin-treated (n = 8) mice. Results are means ± SEM. *B*: Measure of [^{14}C]palmitate incorporation into TG in muscle of PBS-treated (n = 11) and apelin-treated (n = 12) mice. Results are means ± SEM. *C*: Complete (*left*) and incomplete (*right*) FAO measured as described in RESEARCH DESIGN AND METHODS. Results are means ± SEM of PBS-treated (n = 11) and apelin-treated (n = 9) mice. **$P \leq 0.01$.

observed. Increased FAO and mitochondrial biogenesis in muscle and decreased total adiposity could contribute to the overall improvement of insulin sensitivity observed with chronic apelin treatment.

The most inoffensive fate of FAs in skeletal muscle is a matter of debate. Most studies suggest that insulin resistance develops as a consequence of diminished FAO. Instead of being directed to the mitochondria, FAs accumulate as DAG, leading to insulin resistance (28,29). More recently, it has also been suggested that insulin resistance is linked to excessive rather than to reduced FAO and that an overload of FAs in the mitochondria could exert mitochondrial stress, contributing to insulin-desensitizing effects (26). This is thought to result from high rates of incomplete FAO during which partially degraded FAs accumulate as acylcarnitines. Increased levels of acylcarnitines have already been proposed as markers of insulin resistance (26,30), and lower levels of acylcarnitines were shown to reverse HFD-induced glucose intolerance (31). In the current study, apelin treatment increased only the complete FAO and decreased acylcarnitines but not total DAG and IMTG levels in muscle. Improved insulin action in muscle has been observed after exercise intervention without modification of DAG levels (32). As previously suggested, the oxidative capacity in muscle might be a better predictor of insulin sensitivity than TG or DAG content (32). These results suggest that in muscle of HFD insulin-resistant mice treated with apelin, the lipids available to mitochondria do not exceed the capacity for their oxidation.

Impaired fuel oxidation could be attributed to mitochondrial dysfunction, a key factor contributing to insulin resistance (28,33). PGC1 proteins are transcriptional coactivators, considered as key regulators of mitochondrial biogenesis and function (22,34). PGC1-α expression in skeletal muscle is generally decreased during insulin resistance (31,35,36). Moreover, PGC1-α activation could be dependent on AMPK activation to promote mitochondrial biogenesis (25). It was previously shown that rats fed an ND and treated with apelin for 2 weeks had increased mitochondrial content and PGC1-β expression in triceps muscle (37). The current study defines the mechanisms of apelin

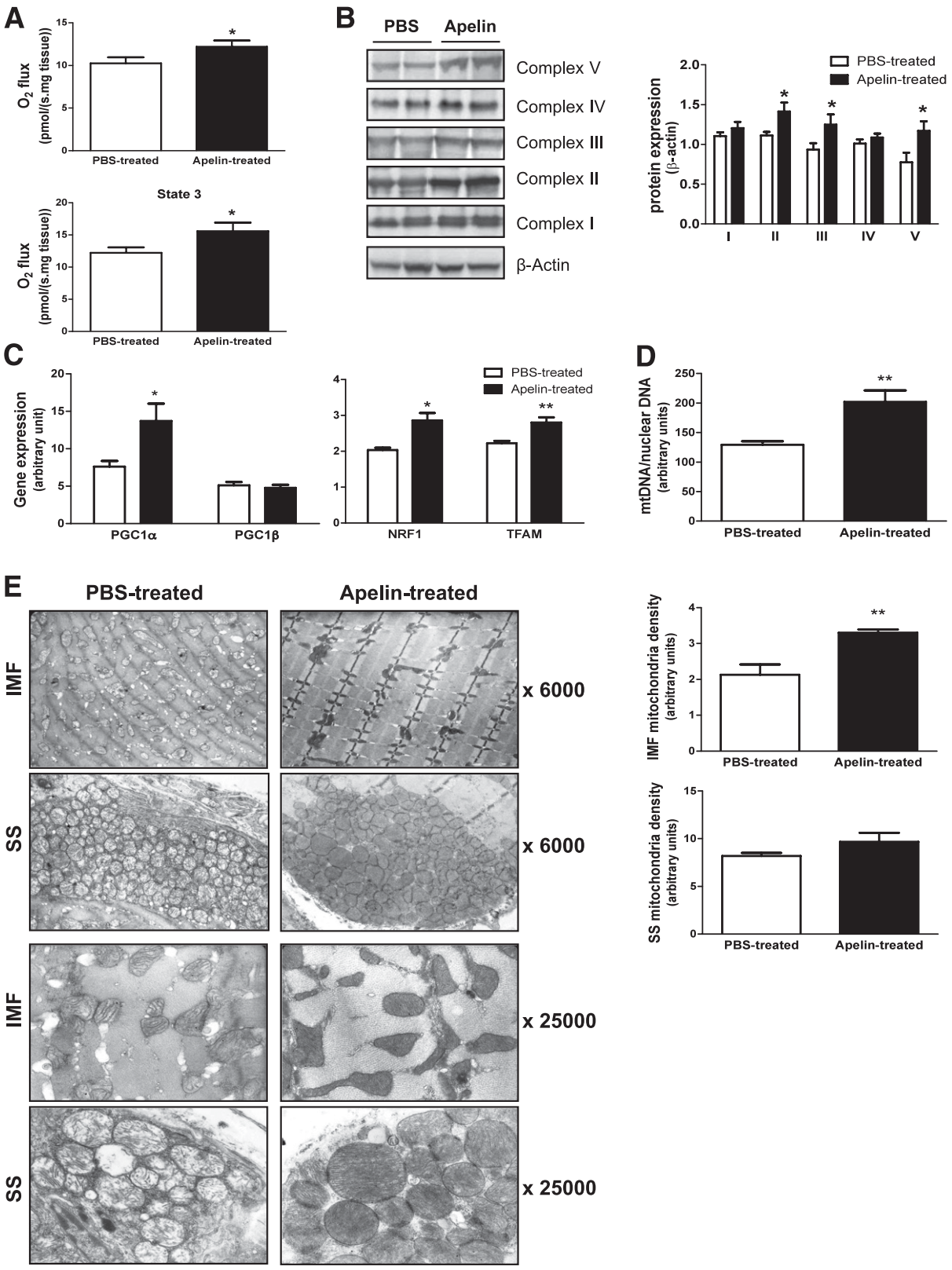


FIG. 4. Chronic apelin treatment in HFD mice increased mitochondrial oxidative capacities and biogenesis in muscle. *A*: State 2 and State 3 respiration were measured on fresh permeabilized fibers prepared from soleus skeletal muscle of PBS-treated (n = 7) and apelin-treated (n = 7) mice as described in RESEARCH DESIGN AND METHODS. *B*: Representative Western blot of the different mitochondrial complexes (*left*) and quantification (*right*) in PBS-treated (n = 6) and apelin-treated (n = 7) mice. Results are means ± SEM. *$P \leq 0.05$. *C*: Gene expression in soleus muscle of PBS-treated (n = 5) and apelin-treated (n = 5) mice. Results are means ± SEM. *$P \leq 0.05$. *D*: mtDNA quantity calculated as the ratio of COX1 to cyclophilin A DNA levels determined by real-time PCR in soleus of PBS-treated (n = 4) and apelin-treated (n = 4) mice. **$P \leq 0.01$. *E*: Transmission electron microscopy images at magnification ×6,000 and ×25,000 in SS and IMF mitochondria (*left*). Quantification of mitochondria number relative to the section area (analysis of three images for each mouse) from soleus of PBS-treated (n = 4) and apelin-treated (n = 5) mice (*right*).

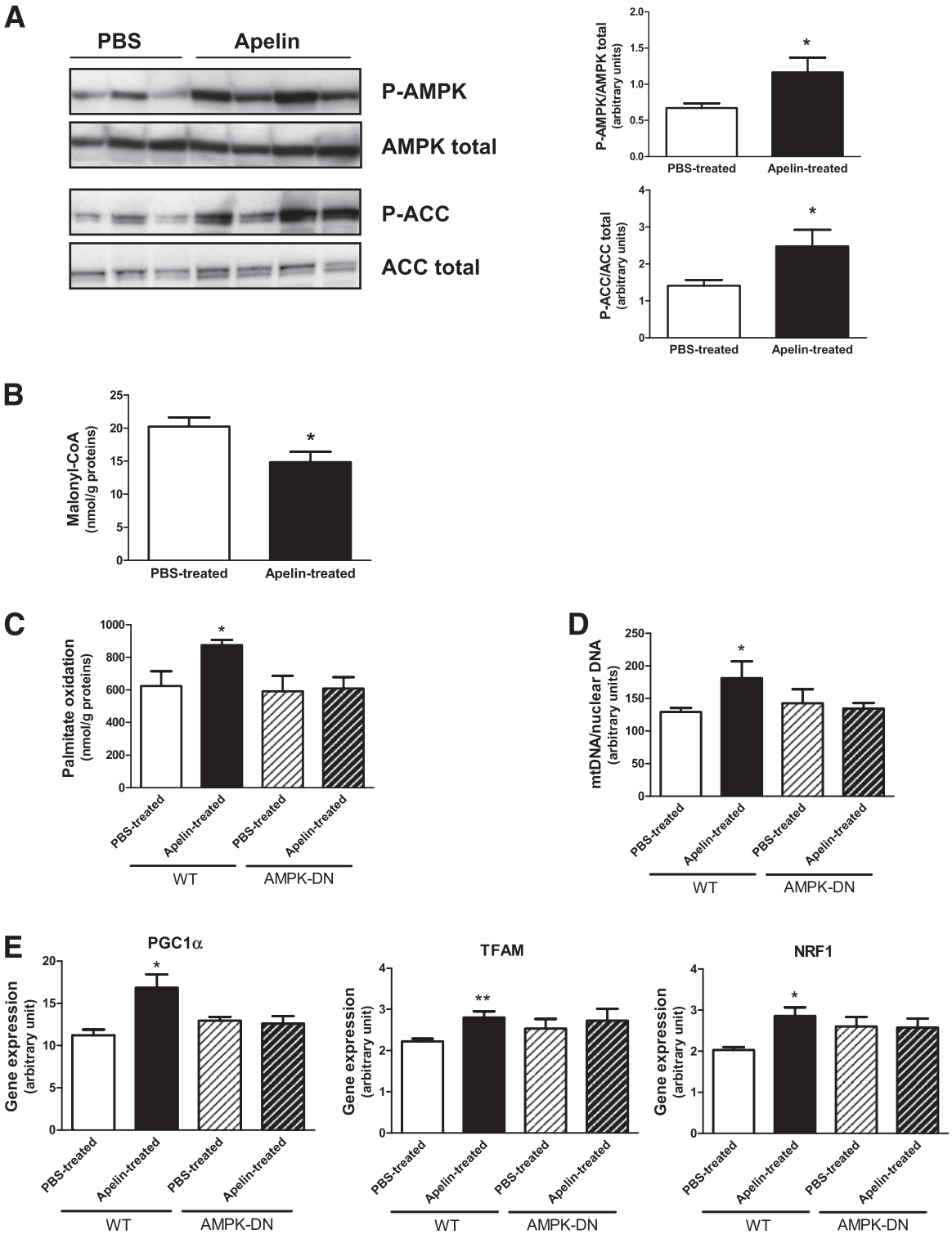


FIG. 5. The effects of apelin on FAO and mitochondrial biogenesis in muscle are dependent on AMPK activation. *A*: Phospho-AMPK and phospho-ACC protein expression after PBS (n = 3) or apelin (n = 4) treatment in muscle of insulin-resistant mice. The graph shows the quantified data (n = 4). *B*: Malonyl-CoA concentration in soleus muscle of PBS-treated (n = 6) or apelin-treated (n = 6) mice. *C*: Total FAO measured as described in RESEARCH DESIGN AND METHODS in HFD PBS- and apelin-treated WT and AMPK-DN mice. Results are means ± SEM; n = 4 in each group. *D*: mtDNA quantity calculated as the ratio of COX1 to cyclophilin A DNA levels determined by real-time PCR in soleus of the different mice; n = 4 in each group. *E*: Gene expression in soleus muscle of PBS- and apelin-treated WT and AMPK-DN mice. Results are means ± SEM; n = 4 in each group. *P < 0.05. **$P \leq 0.01$.

in skeletal muscle in a situation of insulin resistance. We propose that apelin acts through APJ activation to increase AMPK phosphorylation and activity in insulin-resistant skeletal muscle that will inhibit ACC activity and reduced malonyl-CoA levels, leading to increased FAO. Moreover, AMPK activation increased the expression of PGC1-α (but not PGC1-β) as well as its downstream targets NRF1 and TFAM to initiate the replication and transcription of

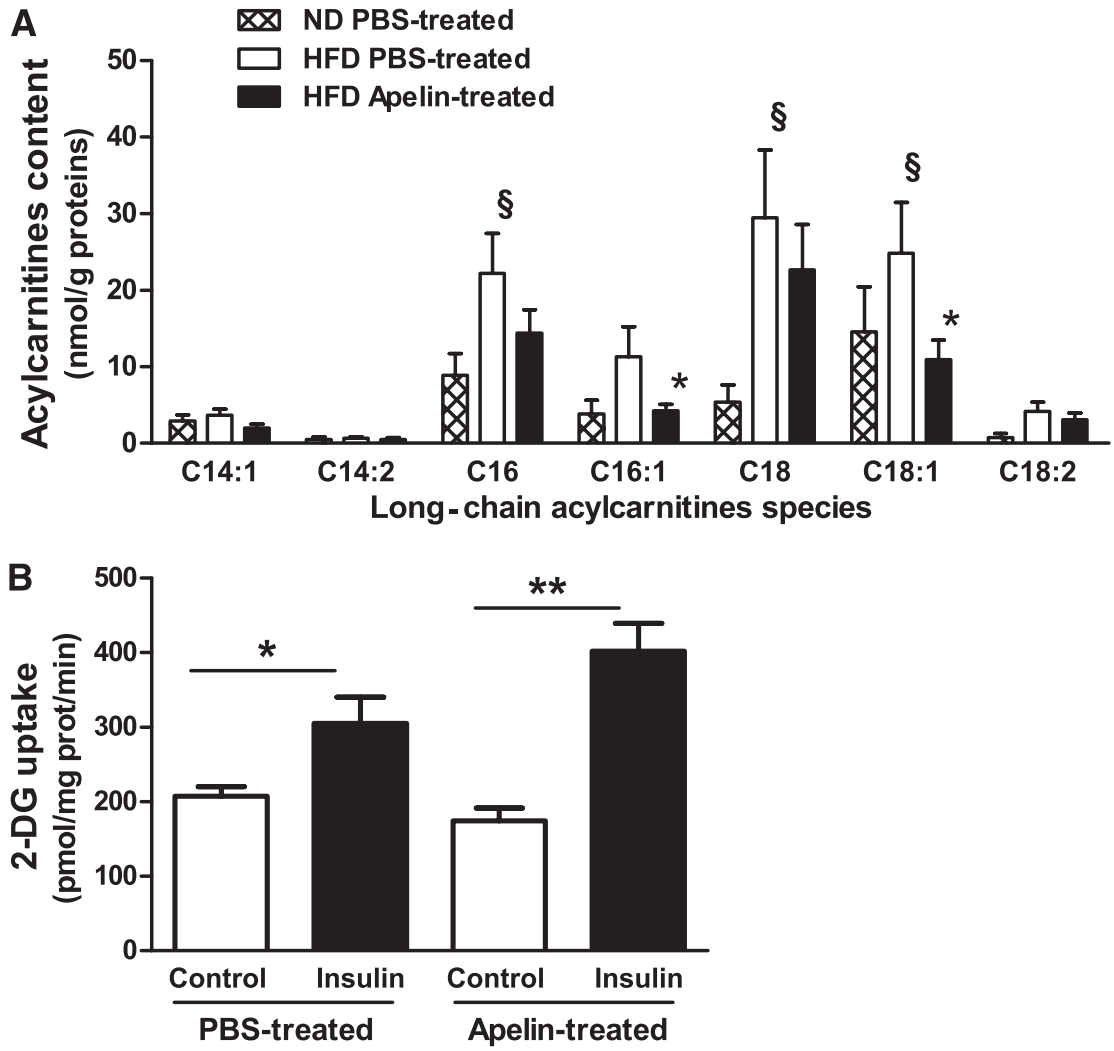


FIG. 6. Effect of chronic apelin treatment in muscle of insulin-resistant mice on acylcarnitine levels and insulin-stimulated glucose uptake. *A*: Long-chain species acylcarnitine levels were measured in ND-fed mice ($n = 5$) and in HFD-fed mice treated with apelin ($n = 8$) or PBS ($n = 7$). Results are means ± SEM. *$P \leq 0.05$. *B*: Insulin-induced glucose uptake in soleus muscle of PBS-treated ($n = 7$) and apelin-treated ($n = 6$) mice. Results are means ± SEM. *$P \leq 0.05$, **$P \leq 0.01$. 2-DG, 2-deoxyglucose; Prot, protein.

mtDNA. Apelin treatment not only increased the density of muscle mitochondria but also improved the ultrastructure of both IMF and SS mitochondria. Increased mitochondrial biogenesis has also been observed in mice overexpressing apelin (38). These events seem to be specific to skeletal muscle since neither FAO nor mitochondrial biogenesis was increased in response to apelin treatment in WAT and brown adipose tissue. Even if apelin has been shown to activate AMPK in WAT (8,9), it can be speculated that AMPK activation regulates substrate flux and whole-body energy distribution accordingly to the tissues as previously reported for other AMPK activators (39).

In this study, accentuated FAO was observed not only in skeletal muscle but also in vivo. Indirect calorimetry experiments showed that HFD apelin-treated mice retained low RER during the dark period (corresponding to feeding period) compared with PBS-treated mice and, thus, relied on lipid oxidation when needed. Apelin$^{-/-}$ mice displayed a lipid oxidation rate during the dark cycle similar to control mice but lacked the metabolic flexibility to increase lipid oxidation during the light cycle (fasted period). This could contribute to the increased adiposity observed in apelin$^{-/-}$ mice. By contrast, a better lipid oxidation in vivo in HFD apelin-treated mice during the dark period could be in line with the observed decreased adiposity and the expression profile of leptin and adiponectin in adipose tissue (Supplementary Fig. 2).

Several events could thus contribute to the improved insulin sensitivity seen in HFD apelin-treated mice. It is already known that apelin$^{-/-}$ mice are insulin resistant, a condition that can be reversed by a 2-week apelin treatment (5). Our results are in agreement with those findings since chronic apelin treatment not only improved overall insulin sensitivity but also increased insulin-stimulated glucose uptake in soleus muscle. Moreover, chronic apelin treatment prevented hyperinsulinemia and reduced hyperglycemia in HFD mice, although plasma leptin and adiponectin were not modified. Thus, the improvement of insulin sensitivity triggered by apelin might be secondary to decreased adiposity but also due to direct action on skeletal muscle. It is likely that chronic apelin treatment improves insulin-stimulated glucose uptake in muscle as a result of increased FAO and limited accumulation of FA intermediates.

In conclusion, chronic apelin treatment triggers an amelioration of both lipid and glucose metabolism. Even

though obese and insulin-resistant mice have enhanced plasma apelin compared with ND mice, adding a bolus of exogenous apelin is beneficial. Chronic apelin treatment optimizes muscle mitochondrial performance through increased mitochondrial biogenesis and a tighter matching between FAO and the tricarboxylic acid cycle. Since mitochondrial dysfunction is now considered a central event in whole-body metabolic dysregulation with regard to type 2 diabetes, apelin treatment appears as an attractive therapeutic strategy.

ACKNOWLEDGMENTS

This work was supported by a grant from Association de Langue Française pour l'Etude du Diabète et des Maladies Métaboliques/Société Francophone du Diabète 2009.

No potential conflicts of interest relevant to this article were reported.

C.A., A.B., and C.D. researched data and contributed to discussion. C.F., S.L.G., D.D., E.W., R.G.-R., and C.R. researched data. V.B. researched data, contributed to discussion, and reviewed and edited the manuscript. K.K. and J.P. contributed to discussion. M.R.-G., T.L., R.B., L.P., and P.V. contributed to discussion and reviewed and edited the manuscript. I.C.-L. contributed to discussion and wrote the manuscript. P.V. and I.C.-L. are the guarantors of this work and, as such, had full access to all the data in the study and take responsibility for the integrity of the data and the accuracy of the data analysis.

The authors thank Prof. Moris Birnbaum (Howard Hughes Medical Institute, University of Pennsylvania, Philadelphia, PA) and Prof. Marc Prentki (Centre Hospitalier de l'Université de Montréal Research Centre [CRCHUM], Montreal, Ontario, Canada) for providing DN-AMPK mice and FA synthetase enzyme, respectively. The authors also acknowledge for their expertise the Anexplo platform (phenotyping and lipidomic and electronic microscopy) and the staff of animal facilities; Claudiane Guay (CRCHUM) for malonyl-CoA assay protocol; Danielle Prévot (INSERM U1048) for excellent technical assistance; Chantal Bertrand (INSERM U1048), PhD student, for her help with experiments for reviewing; and François Crampes and Jean-Sebastien Saulnier-Blache (INSERM U1048) for fruitful discussion and advice.

REFERENCES

1. Boucher J, Masri B, Daviaud D, et al. Apelin, a newly identified adipokine up-regulated by insulin and obesity. Endocrinology 2005;146:1764–1771
2. Tatemoto K, Hosoya M, Habata Y, et al. Isolation and characterization of a novel endogenous peptide ligand for the human APJ receptor. Biochem Biophys Res Commun 1998;251:471–476
3. Carpéné C, Dray C, Attané C, et al. Expanding role for the apelin/APJ system in physiopathology. J Physiol Biochem 2007;63:359–373
4. Dray C, Knauf C, Daviaud D, et al. Apelin stimulates glucose utilization in normal and obese insulin-resistant mice. Cell Metab 2008;8:437–445
5. Yue P, Jin H, Aillaud M, et al. Apelin is necessary for the maintenance of insulin sensitivity. Am J Physiol Endocrinol Metab 2010;298:E59–E67
6. Dray C, Debard C, Jager J, et al. Apelin and APJ regulation in adipose tissue and skeletal muscle of type 2 diabetic mice and humans. Am J Physiol Endocrinol Metab 2010;298:E1161–E1169
7. Higuchi K, Masaki T, Gotoh K, et al. Apelin, an APJ receptor ligand, regulates body adiposity and favors the messenger ribonucleic acid expression of uncoupling proteins in mice. Endocrinology 2007;148:2690–2697
8. Yue P, Jin H, Xu S, et al. Apelin decreases lipolysis via G(q), G(i), and AMPK-dependent mechanisms. Endocrinology 2011;152:59–68
9. Attané C, Daviaud D, Dray C, et al. Apelin stimulates glucose uptake but not lipolysis in human adipose tissue ex vivo. J Mol Endocrinol 2011;46:21–28
10. Kuba K, Zhang L, Imai Y, et al. Impaired heart contractility in Apelin gene-deficient mice associated with aging and pressure overload [corrected in: Circ Res 2008;102:e36]. Circ Res 2007;101:e32–e42
11. Lee DK, Saldivia VR, Nguyen T, Cheng R, George SR, O'Dowd BF. Modification of the terminal residue of apelin-13 antagonizes its hypotensive action. Endocrinology 2005;146:231–236
12. Dyck DJ, Miskovic D, Code L, Luiken JJ, Bonen A. Endurance training increases FFA oxidation and reduces triacylglycerol utilization in contracting rat soleus. Am J Physiol Endocrinol Metab 2000;278:E778–E785
13. Benani A, Barquissau V, Carneiro L, et al. Method for functional study of mitochondria in rat hypothalamus. J Neurosci Methods 2009;178:301–307
14. Knauf C, Cani PD, Ait-Belgnaoui A, et al. Brain glucagon-like peptide 1 signaling controls the onset of high-fat diet-induced insulin resistance and reduces energy expenditure. Endocrinology 2008;149:4768–4777
15. Bonnard C, Durand A, Peyrol S, et al. Mitochondrial dysfunction results from oxidative stress in the skeletal muscle of diet-induced insulin-resistant mice. J Clin Invest 2008;118:789–800
16. Bezaire V, Bruce CR, Heigenhauser GJ, et al. Identification of fatty acid translocase on human skeletal muscle mitochondrial membranes: essential role in fatty acid oxidation. Am J Physiol Endocrinol Metab 2006;290:E509–E515
17. Chace DH, Hillman SL, Van Hove JL, Naylor EW. Rapid diagnosis of MCAD deficiency: quantitative analysis of octanoylcarnitine and other acylcarnitines in newborn blood spots by tandem mass spectrometry. Clin Chem 1997;43:2106–2113
18. Bligh EG, Dyer WJ. A rapid method of total lipid extraction and purification. Can J Biochem Physiol 1959;37:911–917
19. Barrans A, Collet X, Barbaras R, et al. Hepatic lipase induces the formation of pre-beta 1 high density lipoprotein (HDL) from triacylglycerol-rich HDL2. A study comparing liver perfusion to in vitro incubation with lipases. J Biol Chem 1994;269:11572–11577
20. McGarry JD, Stark MJ, Foster DW. Hepatic malonyl-CoA levels of fed, fasted and diabetic rats as measured using a simple radioisotopic assay. J Biol Chem 1978;253:8291–8293
21. Iglesias-Osma MC, Bour S, Garcia-Barrado MJ, et al. Methylamine but not mafenide mimics insulin-like activity of the semicarbazide-sensitive amine oxidase-substrate benzylamine on glucose tolerance and on human adipocyte metabolism. Pharmacol Res 2005;52:475–484
22. Lin J, Handschin C, Spiegelman BM. Metabolic control through the PGC-1 family of transcription coactivators. Cell Metab 2005;1:361–370
23. Patti ME, Corvera S. The role of mitochondria in the pathogenesis of type 2 diabetes. Endocr Rev 2010;31:364–395
24. Witczak CA, Sharoff CG, Goodyear LJ. AMP-activated protein kinase in skeletal muscle: from structure and localization to its role as a master regulator of cellular metabolism. Cell Mol Life Sci 2008;65:3737–3755
25. Reznick RM, Shulman GI. The role of AMP-activated protein kinase in mitochondrial biogenesis. J Physiol 2006;574:33–39
26. Koves TR, Ussher JR, Noland RC, et al. Mitochondrial overload and incomplete fatty acid oxidation contribute to skeletal muscle insulin resistance. Cell Metab 2008;7:45–56
27. Mihalik SJ, Goodpaster BH, Kelley DE, et al. Increased levels of plasma acylcarnitines in obesity and type 2 diabetes and identification of a marker of glucolipotoxicity. Obesity (Silver Spring) 2010;18:1695–1700
28. Morino K, Petersen KF, Shulman GI. Molecular mechanisms of insulin resistance in humans and their potential links with mitochondrial dysfunction. Diabetes 2006;55(Suppl. 2):S9–S15
29. Turner N, Heilbronn LK. Is mitochondrial dysfunction a cause of insulin resistance? Trends Endocrinol Metab 2008;19:324–330
30. Summermatter S, Troxler H, Santos G, Handschin C. Coordinated balancing of muscle oxidative metabolism through PGC-1α increases metabolic flexibility and preserves insulin sensitivity. Biochem Biophys Res Commun 2011;408:180–185
31. Koves TR, Li P, An J, et al. Peroxisome proliferator-activated receptor-gamma co-activator 1alpha-mediated metabolic remodeling of skeletal myocytes mimics exercise training and reverses lipid-induced mitochondrial inefficiency. J Biol Chem 2005;280:33588–33598
32. Bruce CR, Kriketos AD, Cooney GJ, Hawley JA. Disassociation of muscle triglyceride content and insulin sensitivity after exercise training in patients with Type 2 diabetes. Diabetologia 2004;47:23–30
33. Kim JA, Wei Y, Sowers JR. Role of mitochondrial dysfunction in insulin resistance. Circ Res 2008;102:401–414
34. Muoio DM, Koves TR. Skeletal muscle adaptation to fatty acid depends on coordinated actions of the PPARs and PGC1 alpha: implications for metabolic disease. Appl Physiol Nutr Metab 2007;32:874–883

35. Mootha VK, Lindgren CM, Eriksson KF, et al. PGC-1alpha-responsive genes involved in oxidative phosphorylation are coordinately downregulated in human diabetes. Nat Genet 2003;34:267–273
36. Patti ME, Butte AJ, Crunkhorn S, et al. Coordinated reduction of genes of oxidative metabolism in humans with insulin resistance and diabetes: Potential role of PGC1 and NRF1. Proc Natl Acad Sci U S A 2003;100:8466–8471
37. Frier BC, Williams DB, Wright DC. The effects of apelin treatment on skeletal muscle mitochondrial content. Am J Physiol Regul Integr Comp Physiol 2009;297:R1761–R1768
38. Yamamoto T, Habata Y, Matsumoto Y, et al. Apelin-transgenic mice exhibit a resistance against diet-induced obesity by increasing vascular mass and mitochondrial biogenesis in skeletal muscle. Biochim Biophys Acta 2011; 1810:853–862
39. Gaidhu MP, Fediuc S, Ceddia RB. 5-Aminoimidazole-4-carboxamide-1-beta-D-ribofuranoside-induced AMP-activated protein kinase phosphorylation inhibits basal and insulin-stimulated glucose uptake, lipid synthesis, and fatty acid oxidation in isolated rat adipocytes. J Biol Chem 2006;281: 25956–25964